J. Cent. South Univ. (2013) 20: 1341−1353
DOI: 10.1007/s11771-013-1621-9

Springer

Dynamic response characteristics of super high-rise buildings subjected to long-period ground motions

CHEN Qing-jun(陈清军)[1], YUAN Wei-ze(袁伟泽)[1], LI Ying-cheng(李英成)[1], CAO Li-ya(曹丽雅)[2]

1. State Key Laboratory of Disaster Reduction in Civil Engineering (Tongji University), Shanghai 200092, China;
2. Biology and Environment Branch of Jiaxing Vocational and Technical College, Jiaxing 314036, China

Abstract: Spectrum characteristics of different types of seismic waves and dynamic response characteristics of super high-rise building structures under long-period ground motions were comparatively analyzed. First, the ground response wave (named LS-R wave) of a soft soil site with deep deposit, taking long-period bedrock seismic record as input, was calculated by wave propagation method. After that, a TOMAKOMAI station long-period seismic record from the Tokachi-Oki earthquake and conventional El-Centro wave were also chosen. Spectrum characteristics of these waves were analyzed and compared. Then, a series of shaking table tests were performed on a 1:50 scale super high-rise structural model under these seismic waves. Furthermore, numerical simulation of the prototype structure under these excitations was conducted, and structure damages under different intensive ground motions were discussed. The results show that: 1) Spectrum characteristics of ground response wave are significantly influenced by soft soil site with deep deposit, and the predominant period has an increasing trend. 2) The maximum acceleration amplification factor of the structure under the TOM wave is two times that under the El-Centro wave; while the maximum displacement response of the structure under the TOM wave is 4.4 times that under the El-Centro wave. Long-period ground motions show greater influences on displacement responses than acceleration responses for super high-rise building structures. 3) Most inelastic damage occurs at the upper 1/3 part of the super high-rise building when subjected to long-period ground motions.

Key words: long-period ground motion; super high-rise building; shaking table model test; numerical simulation; spectrum characteristic analysis

1 Introduction

Fast population growth and concentrations in urban areas, as a global phenomenon, have resulted in a significant shortage of urban land areas. Therefore, many super high-rise buildings are built in major cities. Fundamental natural periods of these buildings are usually a few seconds. In addition, the long-period ground motion has been clarified from deep-ground surveys and dense seismic observations [1]. Long-period ground motions tend to resonate high-rise buildings, and accordingly the input energy is expected to be several times more than what has been expected in seismic design [2]. Cumulative inelastic deformations would be significantly increased, and severe structural damage may occur. For example, tall and flexible buildings were damaged seriously by long-period ground motions in the Michoacan earthquake (M8.1) in 1985 [3], Wenchuan earthquake (M8.0) in 2011 [4] and Japan earthquake (M9.0) in 2011 [5]. Meanwhile, many large cities such as Shanghai, Guangzhou and Tianjin are located on plains with deep and soft soil. Long-period components of ground motion are amplified when propagating through these sites, resulting in increased damage risk of long-period architectures [6−7].

To this end, the studies in this area have aroused great attention of the academics. Source, path and site effects are influential factors in excitation and propagation of long-period ground motions [8], while good-quality digital long-period seismic records are few for research. Studies are usually focused on displacement and acceleration spectrum [9−10], but the influences of soft soil site with deep deposit on long-period ground motions are not well understood. On the other hand, natural period and damping ratio are two key parameters governing the dynamic response of long-period structures [11]. ARIGA et al [12] investigated the resonant behavior of base-isolated shear high-rise buildings under long-period ground motions. CHUNG et al [13] employed a four-story frame model and added multi-lumped-mass, simulating a 21 storeys building, to study the seismic performance of high-rise buildings. However, seismic response characteristics of super high-

Foundation item: Project(50978198) supported by the National Natural Science Foundation of China; Project(SLDRCE08-B-03) supported by the Ministry of Science and Technology of China
Received date: 2012−02−28; **Accepted date**: 2012−09−20
Corresponding author: YUAN Wei-ze, PhD Candidate; Tel: +86−21−65986185; E-mail: 09ywzcly@tongji.edu.cn

rise buildings subjected to long-period ground motions both from wholly built model tests and detailed numerical analysis have been rarely reported so far.

In this work, a ground response wave (LS-R wave) of soft soil site with deep deposit, a typical long-period ground motion record (TOM wave) and a conventional seismic wave (El-Centro wave) were selected as the input excitations. Spectrum characteristics of these waves were analyzed and compared. After that, a series of shaking table tests were carried out on a 1:50 scale super high-rise building model to explore its performance under these excitations. Furthermore, a finite element model of the prototype structure was established. The responses obtained from numerical model were compared with the test results. Then, damage analysis of the prototype structure under amplified input ground motions was conducted.

2 Selection and analysis of input seismic waves

2.1 Ground response wave

According to the soil exploration information and current Shanghai foundation norms, HUANG et al [14−15] designed a typical geological section. This model was adopted for the ground response analysis of soft soil site with deep deposit by one-dimensional equivalent linear wave propagation method [16]. Considering the dynamic properties of sandy soil and cohesive soil, Seed-Sun model and Seed-Idriss model were prepared to study the decline curves between modulus-ratio and shearing strain, respectively. Table 1 lists the values of shear modulus (G/G_{max}) and damping ratio (D) for sandy soil and cohesive soil with the variation of shear strain (λ).

Table 1 Equivalent model of shearing modulus and damping ratio

λ/%	Sandy soil		Cohesive soil	
	G/G_{max}	D%	G/G_{max}	D%
0.0001	1	0.24	1	0.24
0.0003	1	0.42	1	0.42
0.001	0.99	0.8	1	0.8
0.003	0.96	1.4	0.981	1.4
0.01	0.85	2.8	0.941	2.8
0.03	0.64	5.1	0.847	5.1
0.1	0.37	9.8	0.656	9.8
0.3	0.18	15.5	0.428	15.5
1	0.08	21	0.238	21
3	0.05	25	0.144	25
10	0.035	28	0.11	28

The input bedrock seismic record (named HKD123 wave) is the N-S component of HKD123 station recorded during the Tokachi-Oki earthquake (M8.0) in 2003, which has typical long-period characteristics. The epicenter is 240 km, and the site condition is bedrock. Figure 1 shows the time histories, Fourier spectra and velocity response spectra of HKD123 wave and LS-R wave. Apparently, Fig. 1 shows that: 1) The mid and low frequency components of HKD123 wave are magnified by deep and thick soft clay ground, while the high frequency components are attenuated badly. 2) The predominant period of LS-R wave (2.35 s) is larger than that of HKD123 wave (1.17 s), which indicates that the predominant period of ground response wave has an increasing trend.

2.2 Long-period seismic wave and conventional seismic wave

Long-period TOM wave is the E-W component of HKD129 station recorded during the Tokachi-Oki earthquake (M8.0) in 2003. The epicenter is 238 km, and the site condition is Type IV soft soil. Conventional El-Centro wave (as the comparative seismic wave) is the E-W component recorded during the California Imperial Valley earthquake (M6.7) in 1940. The epicenter is 11.5 km, and the site condition is Type II−III. Figure 2 shows the time histories, Fourier spectra and velocity response spectra of them, which illustrates that: 1) TOM wave has the characteristics of small acceleration amplitude, long duration, plenty of low frequency components and main frequency distributing between 0.15 and 1 Hz. On the contrary, the characteristics of El-Centro wave are obviously opposite and the main frequency distributing is 0.20−4 Hz. 2) The predominant period of TOM wave is 7.04 s and the distribution of spectrum value is broad in periodic domain, while the predominant period of El-Centro wave is 2.10 s and the spectrum value is mainly distributed within 6.0 s.

2.3 Input energy spectra of seismic excitations

For further investigating the characteristics of seismic excitations, the input energy spectra [17] are calculated with PGA of 20 gal and shown in Fig. 3. It can be seen from Fig. 3 that: 1) The peak values of TOM wave and LS-R wave are 0.178 m^2/s^2 and 0.152 m^2/s^2, respectively, which are much larger than those of El-Centro wave. 2) The input energy of TOM wave is mainly distributed between 4 and 10 s, while that of LS-R wave is 2−3 s.

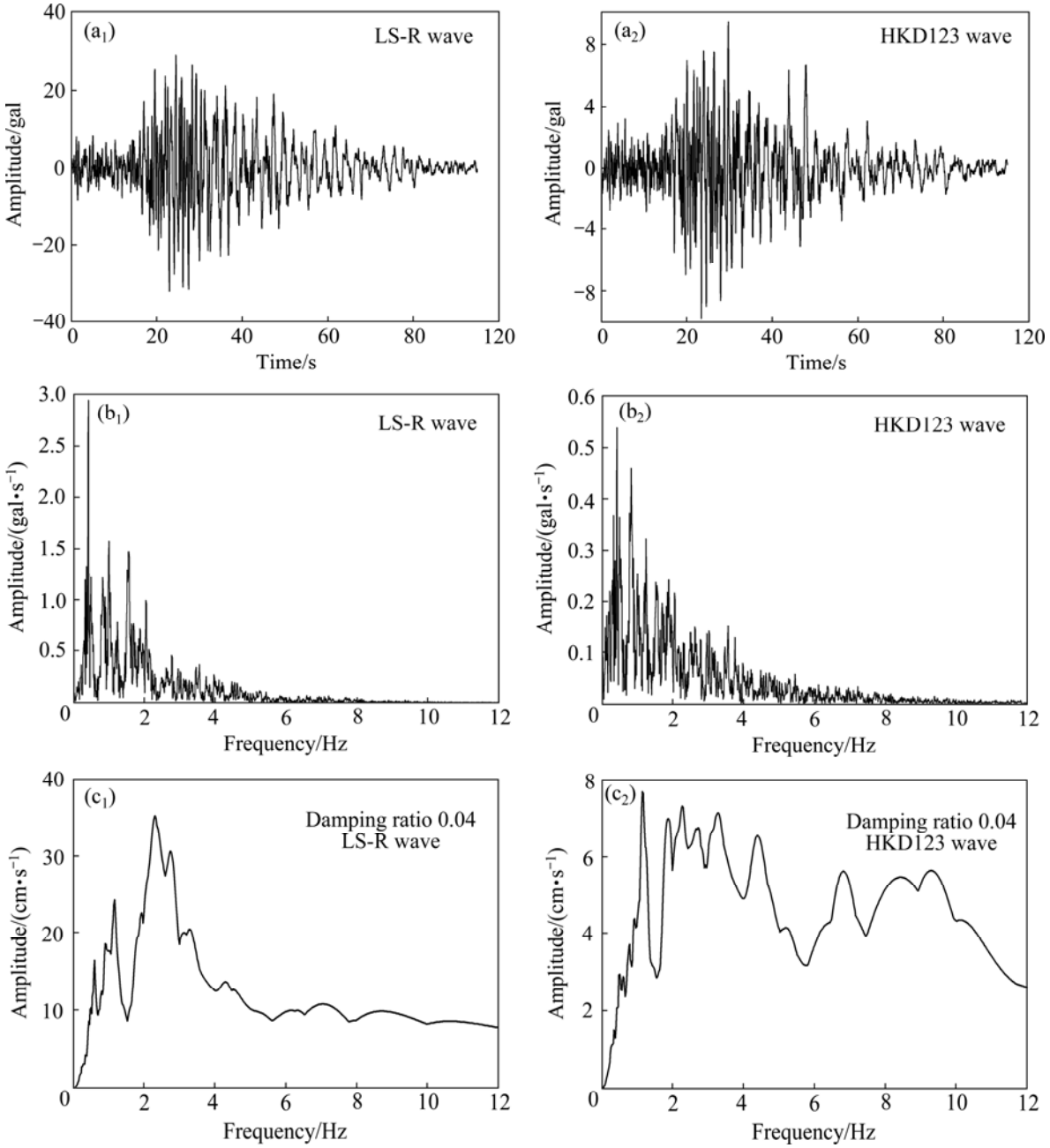

Fig. 1 Comparison between HKD123 wave and LS-R wave: (a) Time histories; (b) Fourier spectra; (c) Velocity response spectra

3 Shaking table test

3.1 General information of prototype structure

The prototype structure is a multifunctional skyscraper. The main structure height is 580 m and top height is 632 m, and the area of whole building is about 4.2×10^7 m^2. The building is divided into eight zones and an observation deck, and mechanical floor and refuge storey are arranged at the top of each zone. Figure 4 shows the structure plan view of standard floor. Table 2 lists the parameters of columns and core-tube.

3.2 Test model description and testing procedure

The similitude relationships are listed in Table 3. According to the purpose of experiment, the test model was partially simplified on the basis of theoretical analysis and contrast calculation. The model structure was placed at a rigid beam base with height of 0.4 m and mass of 4.082 t. The height and mass of the model were about 12.64 m and 24.97 t, respectively. More information about the test model can be found in Ref. [18].

There were two types of inputs: 3D synthesized white noise and 1D earthquake inputs. Before the inputs of each event, a 3D white noise was first input to acquire

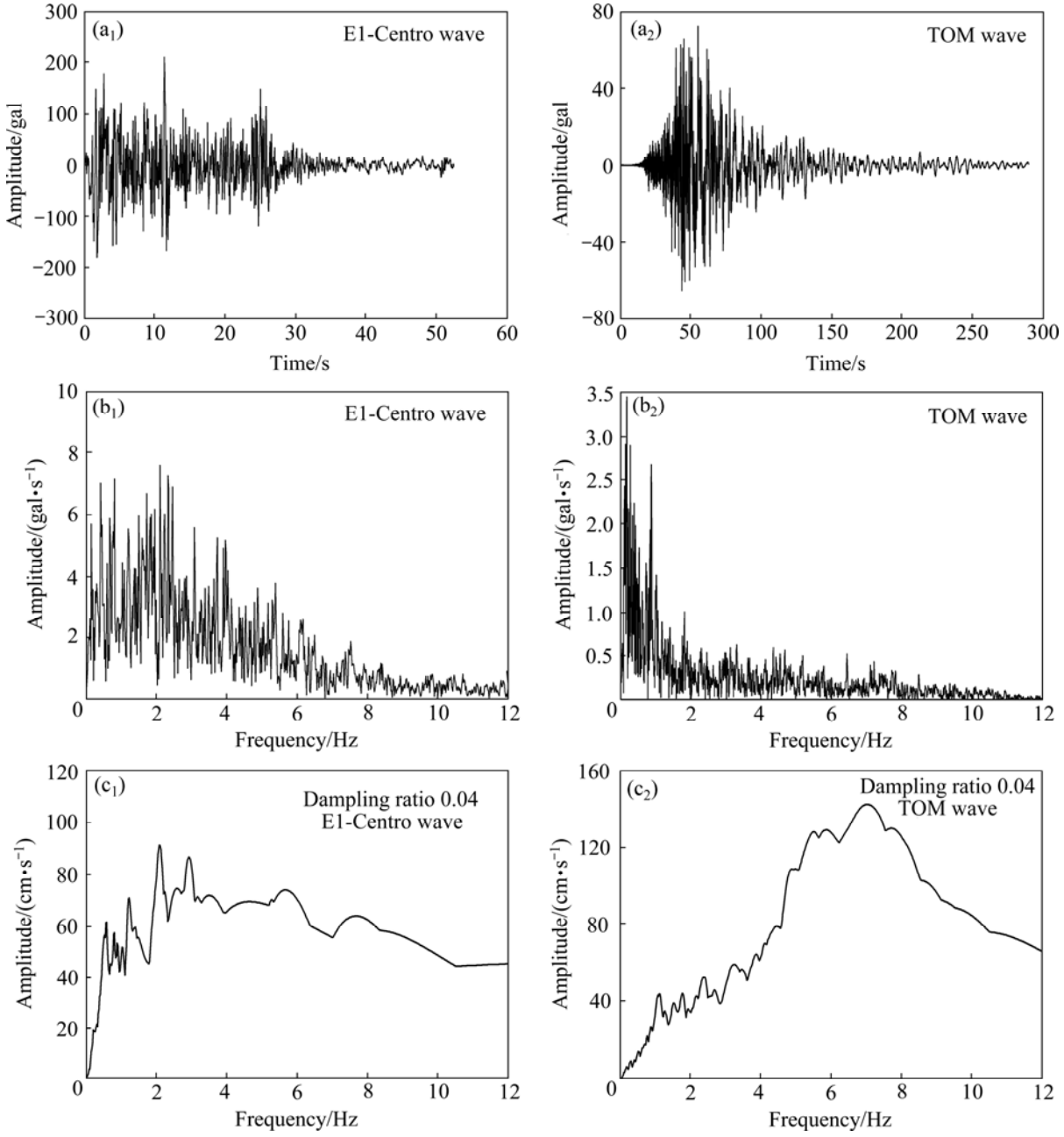

Fig. 2 Comparison between TOM wave and El-Centro wave: (a) Time histories; (b) Fourier spectra; (c) Velocity response spectra

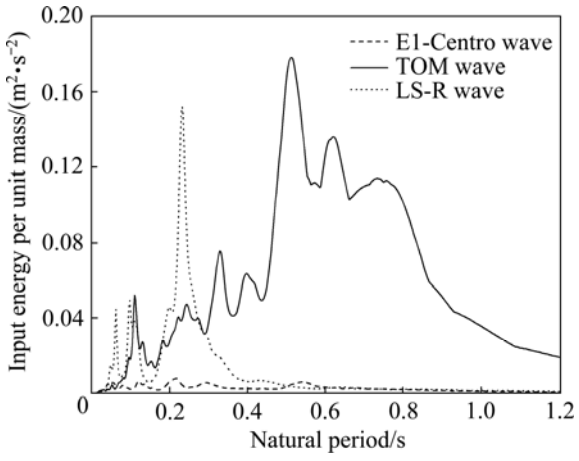

Fig. 3 Input energy spectra of seismic excitations

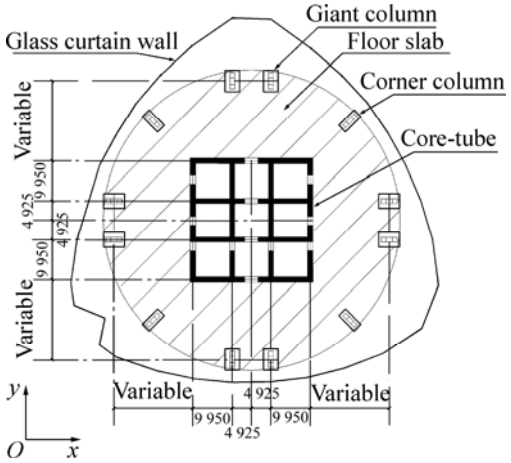

Fig. 4 Structural plan of standard floor (Unit: mm)

Table 2 Parameters of columns and core-tube

Zone number	Cross section of giant column/m	Cross section of corner column/m	Concrete strength grade	Wing wall thickness of core-tube/m	Web wall thickness of core-tube/m	Concrete strength grade
8	1.9×2.4	—	C50	0.60	0.50	C60
7	2.3×3.3	—	C50	0.60	0.50	C60
6	2.5×4.0	—	C60	0.60	0.60	C60
5	2.6×4.4	1.2×4.5	C60	0.70	0.65	C60
4	2.8×4.6	1.5×4.8	C60	0.80	0.70	C60
3	3.0×4.8	1.8×4.8	C70	1.00	0.80	C60
2	3.4×5.0	2.2×5.0	C70	1.20	0.90	C60
1	3.7×5.3	2.4×5.5	C70	1.20	0.90	C60

Table 3 Similitude between model and prototype

Physical parameter	Length	Time	Frequency	Density	Elastic modulus	Strain	Acceleration
Similitude relationship	S_l=1/50	S_t=0.077	S_f=12.96	S_ρ=3.87	S_E=0.26	S_ε=1	S_a=3.36

the dynamic behavior of the model. Simulations of El-Centro wave, LS-R wave and TOM wave were then input to the model in turn. Each ground motion simulation was input twice: once in the principal direction *X* and once in direction *Y*. Note that the shaking table test is a supplementary experiment after routine tests and it is a nondestructive test, so the strength of input seismic waves is relatively low. The PGA of input seismic waves was adjusted to 20 gal and the PGA multiplied by the acceleration scaling factor (S_a in Table 3) was used to obtain the target input peak values.

3.3 Test results

3.3.1 Model dynamic properties

From transfer functions obtained from the recorded acceleration responses to white noise [19], the dynamic properties were calculated. The natural frequencies and damping ratios are listed in Table 4, and some mode shapes are shown in Fig. 5.

Table 4 Summary of test result from white noise vibration

Serial number	Frequency/Hz	Damping ratio
1	1.39	0.038 0
2	1.50	0.056 0
3	2.57	0.030 0
4	4.18	0.017 0
5	4.18	0.012 0
6	4.74	0.047 0
7	7.07	0.048 0
8	7.55	0.055 0
9	8.58	0.065 0

3.3.2 Acceleration responses

The amplification factor of acceleration is an important index reflecting the structural dynamic responses. The amplification factor of acceleration at floor *i* is defined as

$$\alpha_i = \frac{\max(\ddot{x}_i(t))}{\max(\ddot{x}_g(t))} \tag{1}$$

where $\ddot{x}_g$ is the time history of acceleration at the shaking table, and $\ddot{x}_i$ is the time history of acceleration at the floor *i*. Figure 6 plots the acceleration amplification factor under different ground motions. Note that the acceleration amplification factor varies weakly with height of the main structure, but increases dramatically at the top observation deck. This phenomenon indicates that: 1) Due to the stiffening effect of storey with outriggers and belt members, the stiffness is evenly distributed along the main structure. 2) Whiplash effect on the top observation deck of the test model is obviously observed. The maximum acceleration amplification factors of the test model are 10.12 in direction *X* and 8.57 in direction *Y* under TOM wave, which are about 2.0 times and 1.6 times those under El-Centro wave, respectively.

3.3.3 Displacement responses

Figure 7 shows the maximum inter-storey displacements under different ground motions. The maximum displacement responses are slightly different in both directions, but there is an obvious growing tendency with floor height under long-period ground motion. The maximum displacement responses of the test model are 14.83 mm in direction *X* and 13.70 mm in direction *Y* under TOM wave, which are about 4.4 times and 4.1 times those under El-Centro wave, respectively.

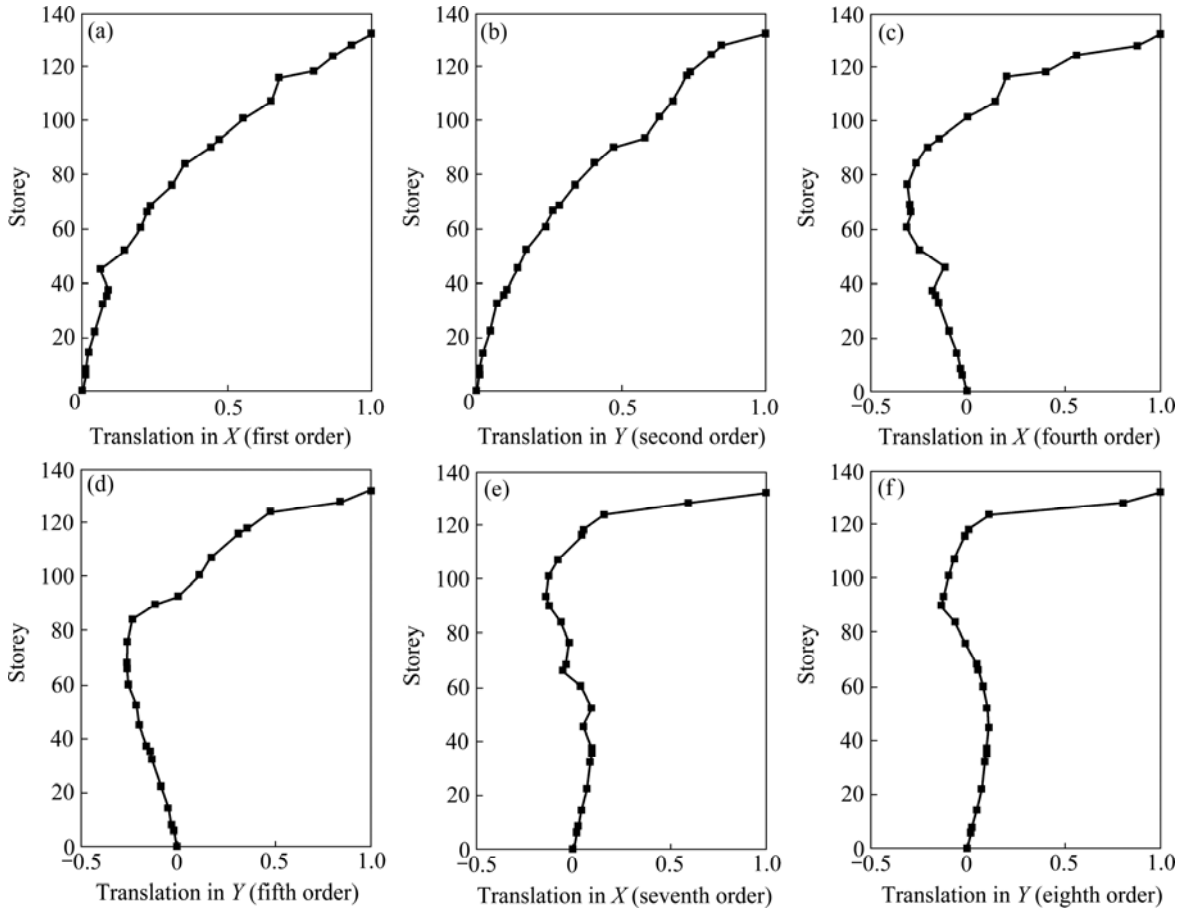

Fig. 5 Vibration modes of test model: (a) First order; (b) Second order; (c) Fourth order; (d) Fifth order; (e) Seventh order; (f) Eighth order

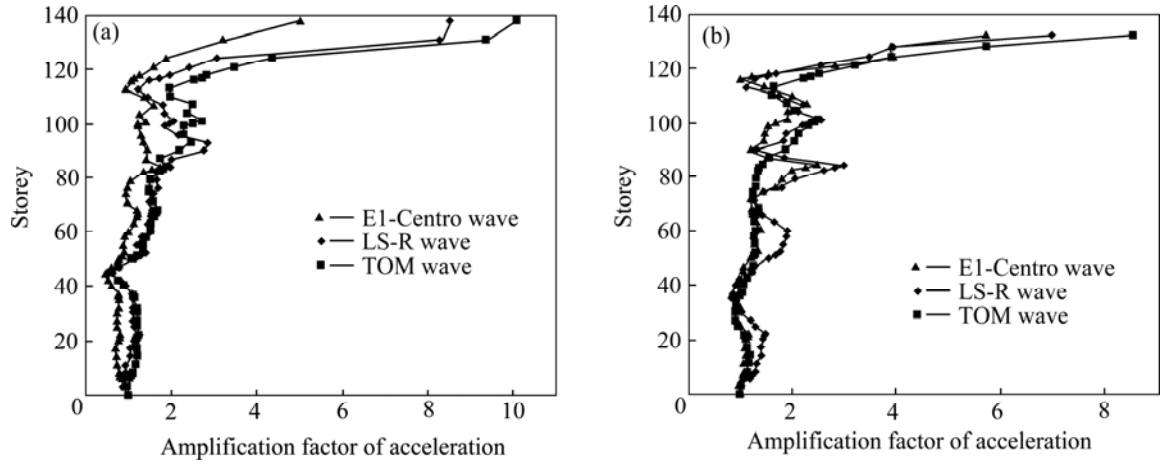

Fig. 6 Acceleration amplification factor envelopes of test model: (a) Direction *X*; (b) Direction *Y*

From the comparison between acceleration responses and displacement responses of the test model, it can be found that displacement responses increase significantly under long-period ground motion.

3.3.4 Inner force responses

Figure 8 summarizes floor shear force and overturning moment of the test model under various excitations. Note that the floor shear force and overturning moment of the test model under long-period ground motion, especially TOM wave, are larger than the results under conventional ground motion. The base shears triggered by TOM wave are 2.6 times in direction *X* and 2.2 times in direction *Y* of those triggered by El-Centro wave, respectively. The base moments caused by TOM wave are 3.3 times in direction *X* and 3.0 times in direction *Y* of those caused by El-Centro wave, respectively.

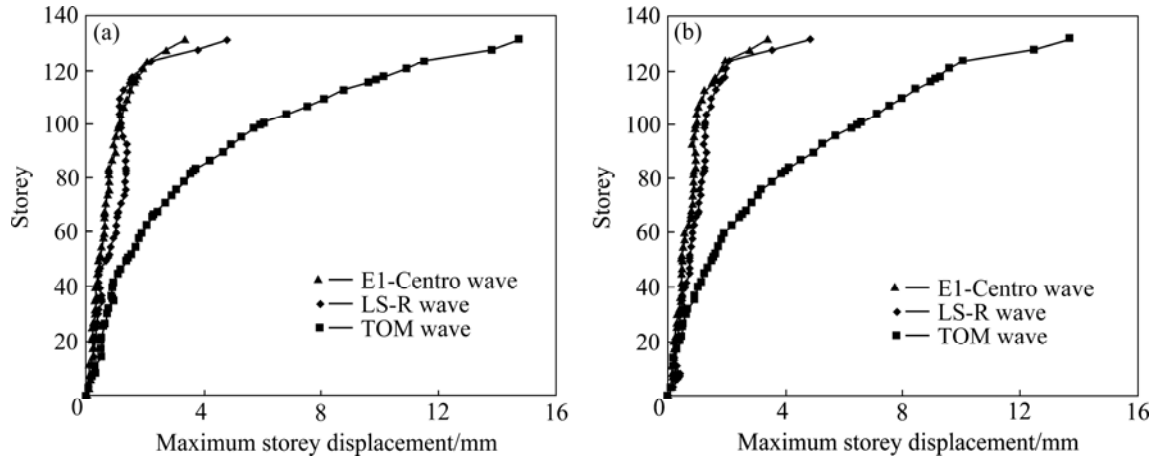

Fig. 7 Maximum storey displacements of test model: (a) Direction *X*; (b) Direction *Y*

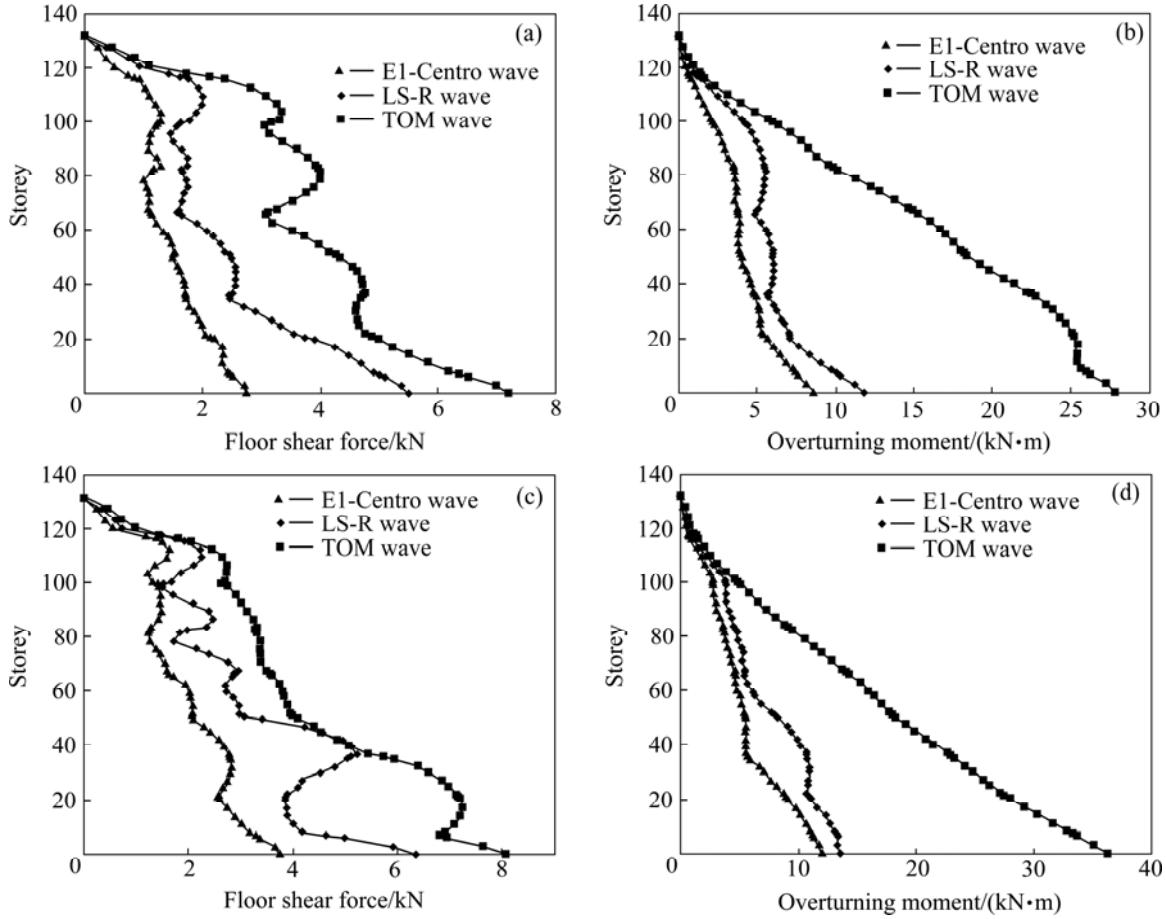

Fig. 8 Floor shear force and overturning moment diagrams of test model: (a), (b) Direction *X*; (c), (d) Direction *Y*

Comparison between the base shear and base moment indicates that long-period ground motion tends to have a greater impact on base moment of super high-rise structures than base shear.

4 Numerical analysis

To make further research about the seismic response of the super high-rise structure, 3D finite element analysis software (ABAQUS) was used to analyze the prototype structure.

4.1 Analytical model and dynamic behavior of prototype structure

Figure 9 shows the numerical model of the prototype structure, in which geometric and material nonlinearities were considered. Beam elements (B32) and PQ-FIBER model [20] were selected for columns.

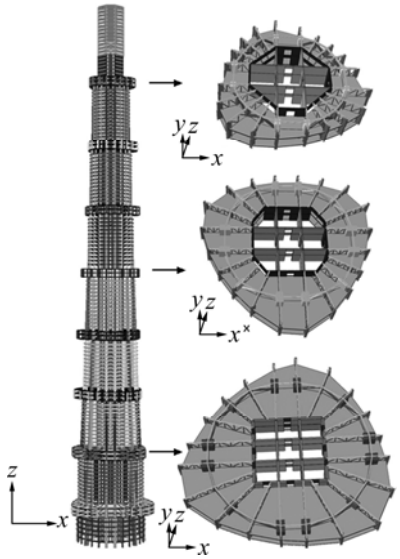

Fig. 9 Numerical model of prototype structure

Shell elements (S4R) and concrete damaged plasticity model were employed for shear wall and coupling beam. A bilinear kinematic hardening material law was selected for steel members and reinforcement bar (yield stress f_y=345 MPa), and the tangent modulus E_1 equaled 0.02E (E is the elastic modulus). Material properties were calculated according to code GB50010 [21]. Basement was assumed to be rigid, and damping ratio calculated from test results was adopted in the analysis.

After mode analysis of the numerical model, natural period and mode shapes were obtained. Table 5 lists the natural period of numerical model, test prototype (from reciprocal of natural frequencies of test model multiplying S_f in Table 3) and Ref. [22]. Considering that the test model was partially simplified, test error of fundamental period of the numerical model is less than 2.4% away from the test prototype but very close to the result of Ref. [22], which can verify the accuracy and efficiency of the numerical model. The first nine mode shapes are shown in Fig. 10.

4.2 Comparative analysis

The responses of prototype structure can be obtained by test results [23]. In this section, the test model responses are first extrapolated to work out the responses of prototype structure, then comparative studies are implemented based on the results of shaking table test and numerical analysis. Some typical calculated responses compared with the test results are shown in Figs. 11 and 12. The letters P and N denote prototype structure and numerical model, respectively. Note that there are some discrepancies between measured and calculated results, which can be interpreted as follows: 1) Fabrication errors of the test model; 2) Measurement noise during tests; 3) Simplifications of the numerical model. However, the overall comparisons indicate that the discrepancies are acceptable.

It is apparent from Figs. 11 and 12 that: 1) The variation of acceleration amplification factor, maximum storey displacement and inter-storey drift of the prototype structure show similar trend both under long-period seismic waves and conventional seismic waves. 2) However, the influence of long-period ground motions on displacement response is significantly greater

Table 5 Comparison of natural period (s)

Model	T_1	T_2	T_3	T_4	T_5	T_6	T_7	T_8	T_9
Numerical model	9.12	9.03	4.33	3.02	2.98	2.10	1.77	1.63	1.60
Test prototype	9.34	8.66	5.05	3.10	3.10	2.74	1.83	1.72	1.51
Model of Ref. [22]	9.10	9.04	4.11	3.09	3.05	1.97	−	−	−

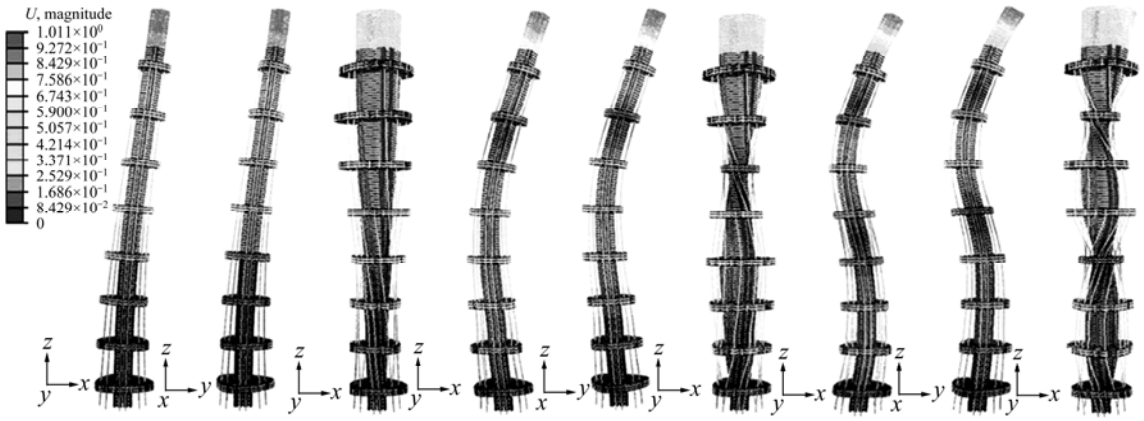

Fig. 10 First nine mode shapes of numerical model

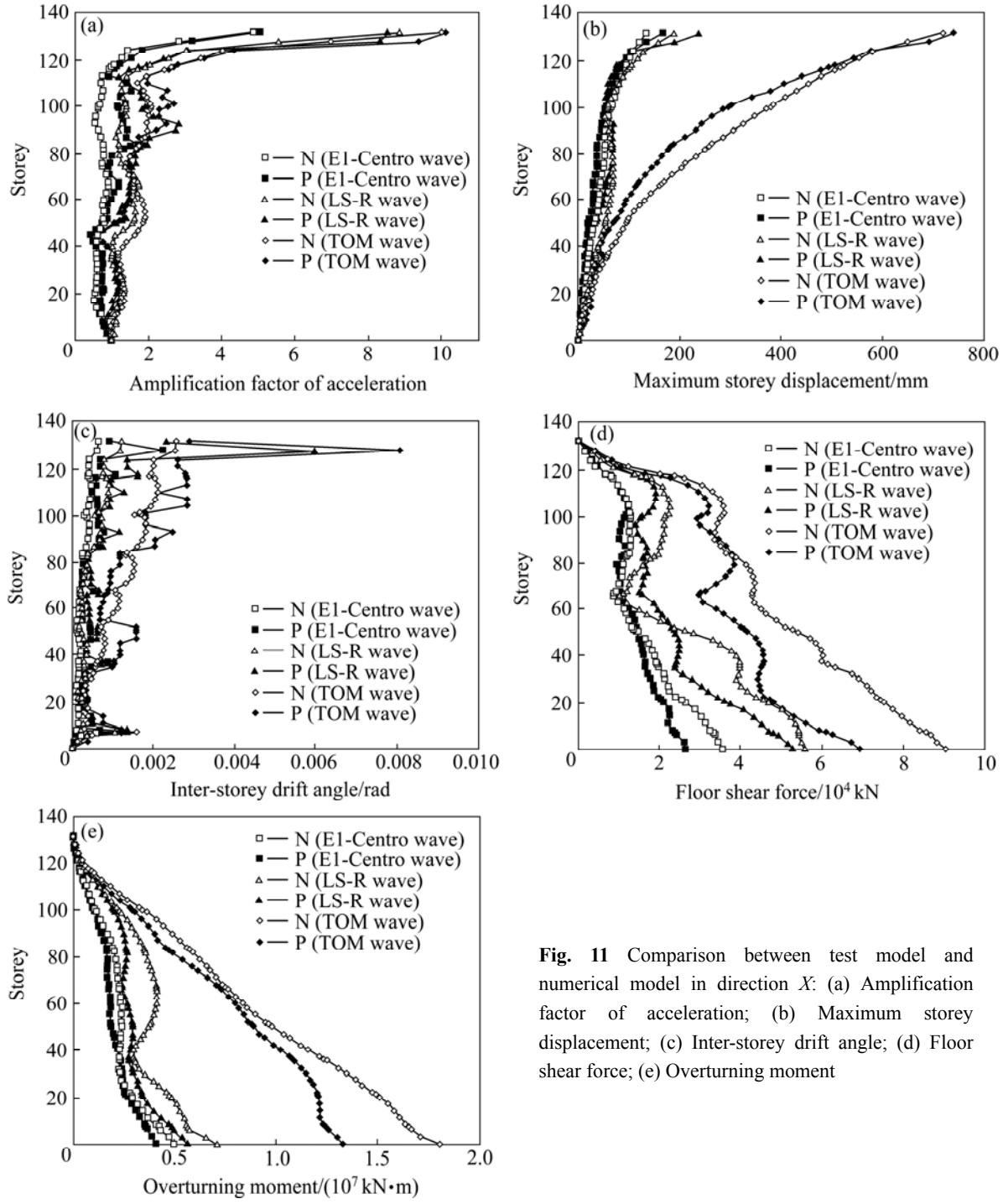

Fig. 11 Comparison between test model and numerical model in direction *X*: (a) Amplification factor of acceleration; (b) Maximum storey displacement; (c) Inter-storey drift angle; (d) Floor shear force; (e) Overturning moment

than that of acceleration response, demonstrating that the displacement response triggered by long-period ground motions is the primary control factor in super high-rise building design.

4.3 Damage analysis

Seismic damage mechanism of structures can be explained more clearly by dynamic analysis based on the energy concept. The dynamic equilibrium equation of motion under seismic excitation is

$$\boldsymbol{M}\ddot{\boldsymbol{X}}(t)+\boldsymbol{C}\dot{\boldsymbol{X}}(t)+\boldsymbol{K}\boldsymbol{X}(t)=-\boldsymbol{M}\ddot{\boldsymbol{X}}_{\mathrm{g}}(t) \tag{2}$$

where $\boldsymbol{M}$ is the mass matrix, $\boldsymbol{C}$ is the damping matrix, $\boldsymbol{K}$ is the stiffness matrix, $\dot{\boldsymbol{X}}(t)$ is the velocity vector, $\ddot{\boldsymbol{X}}(t)$ is the acceleration vector, and $\ddot{\boldsymbol{X}}_{\mathrm{g}}(t)$ is the ground acceleration vector.

Integrating both sides of the equation from time zero to time t_k, the energy balance equation is obtained, i.e.,

$$W_{\mathrm{e}}+W_{\mathrm{h}}+W_{\mathrm{s}}+W_{\mathrm{p}}=E_{\mathrm{i}} \tag{3}$$

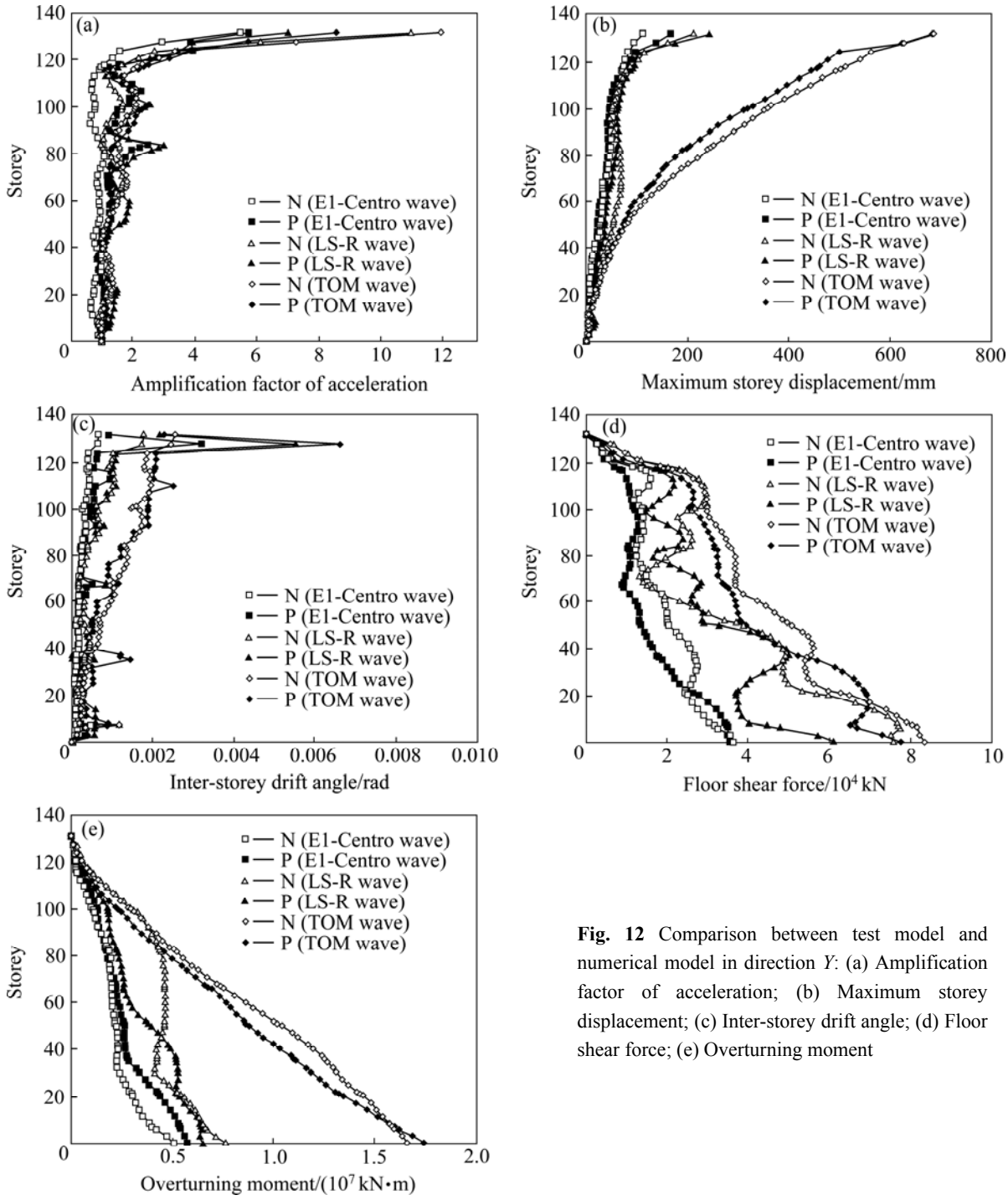

Fig. 12 Comparison between test model and numerical model in direction *Y*: (a) Amplification factor of acceleration; (b) Maximum storey displacement; (c) Inter-storey drift angle; (d) Floor shear force; (e) Overturning moment

where $E_i = -\int_0^{t_k} \dot{\boldsymbol{X}}^T \boldsymbol{M}\ddot{\boldsymbol{X}}_g \mathrm{d}t$, is the input energy; $W_e = \int_0^{t_k} \dot{\boldsymbol{X}}^T \boldsymbol{M}\ddot{\boldsymbol{X}}\mathrm{d}t$, is the kinetic energy; $W_h = \int_0^{t_k} \dot{\boldsymbol{X}}^T \boldsymbol{C}\dot{\boldsymbol{X}}\mathrm{d}t$, is the damping energy; W_s is the elastic strain energy, W_p is the plastic energy, and $W_s + W_p = \int_0^{t_k} \dot{\boldsymbol{X}}^T \boldsymbol{K}\boldsymbol{X}\mathrm{d}t$, is the total deformation energy. The existence of plastic energy (W_p) in the equation is an indicator of the damage of the structure due to earthquake ground motion. It represents the energy that is consumed by the plastic deformation in the structure at time t_k. The larger the value of W_p is, the more significant the damage has been caused by the earthquake.

Table 6 lists the plastic energy and input energy of the structure under three amplified ground motions in direction *X*. It can be observed that: 1) When PGA keeps the same, the input energy of TOM wave is much more than other waves, which is coincident with the input energy spectra of the seismic excitations; 2) The structure entered elasto-plastic state under LS-R wave

and TOM wave with PGA of 0.05*g*, but the responses of the structure became nonlinear under El-Centro wave with PGA of 0.10*g*; 3) When PGA keeps the same, the plastic energy of the structure under TOM wave is more than that of other waves, which shows that the structure has been damaged more seriously by long-period ground motions.

Table 6 Plastic energy and input energy of structure under different ground motions (kJ)

PGA/*g*	El-Centro wave		LS-R wave		TOM wave	
	W_p	E_i	W_p	E_i	W_p	E_i
0.05	0	5 305	88	78 929	353	227 484
0.10	39	31 071	475	175 418	4 012	910 630
0.15	97	93 594	2 174	394 795	34 727	2 056 710

Figure 13 shows the distribution of concrete tensile and compression damage of the core-tube under TOM wave with PGA of 0.15*g*. It can be observed that: 1) The concrete of main structure has been damaged by the ground motion; 2) The positions of concrete tensile and compression damage locate in the upper part of structure, especially at the 6th, 7th and 8th zones.

The maximum displacement, maximum inter-storey drift angle, base shear and base moment of the structure under three ground motions with PGA of 0.15*g* in direction *X* are shown in Table 7. It can be seen that the response values under long-period ground motions are lager than those under El-Centro wave. The maximum displacement response under TOM wave is about 10.4 times more than that under El-Centro wave, which indicates that the displacement response triggered by long-period ground motion is the main factor in super high-rise buildings damage.

Figure 14 shows the distribution of inter-storey drift angles under different grounds with PGA of 0.15*g*. Note that: 1) The inter-story drift angles of the structure under TOM wave are larger than those under El-Centro wave and LS-R wave. 2) The positions of the maximum inter-story drift angles locate in the 7th and 8th zones, which agrees well with the distribution of core-tube damage. Distributions of the maximum inter-storey drift angles and structure damage indicate that long-period ground motion has more influence on the upper 1/3 part of the super high-rise building, thus careful treatment is necessary in the structural design.

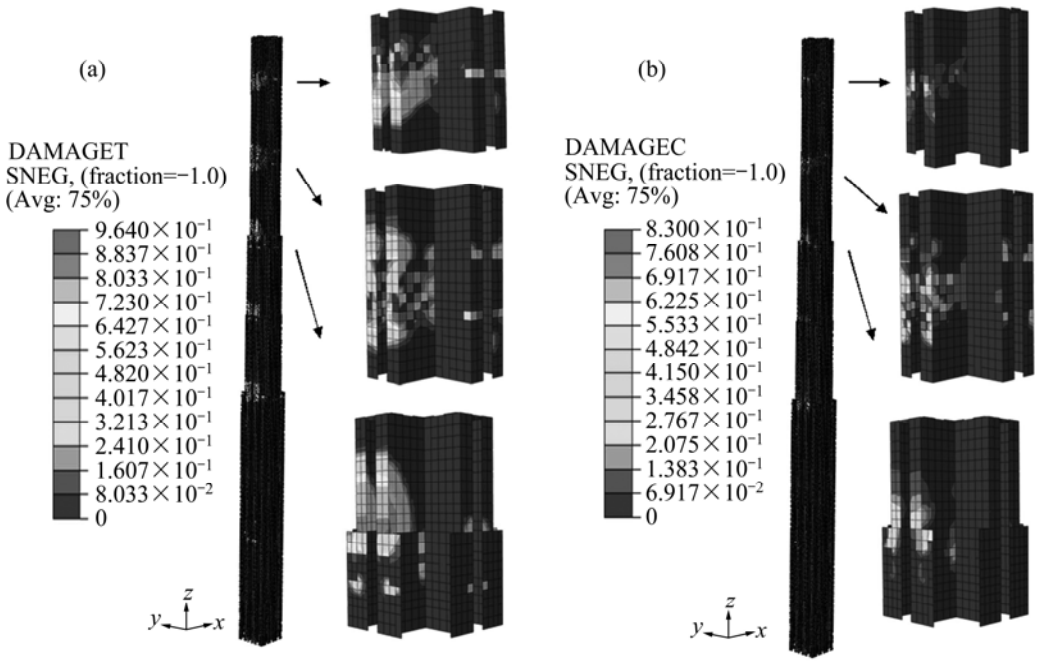

Fig. 13 Concrete damage of main structure: (a) Tensile damage; (b) Compression damage

Table 7 Maximum displacement, maximum inter-story drift angle, base shear and base moment of structure

Seismic wave	Maximum displacement/mm	Maximum inter-storey drift angle	Base shear/10^5kN	Base moment/(10^7kN·m)
El-Centro	269.8	1/806	1.21	0.89
LS-R	618.2	1/283	2.78	2.72
TOM	2 812.5	1/115	4.58	7.44

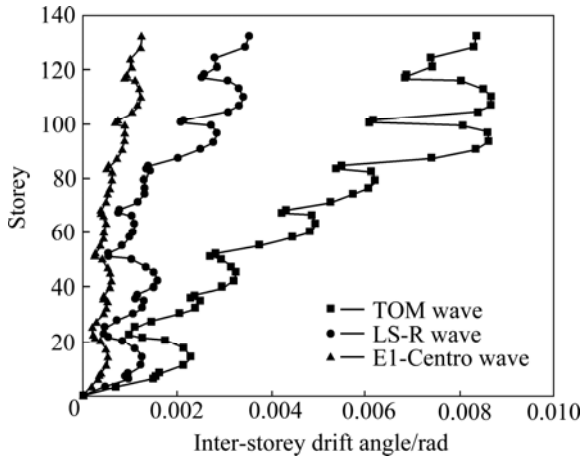

Fig. 14 Distribution of inter-storey drift angle

5 Conclusions

1) Spectrum characteristics of ground response wave are significantly influenced by soft soil site with deep deposit, the mid and low frequency components are magnified, while the high frequency components are attenuated badly. The predominant period of ground response wave has an increasing trend.

2) The maximum acceleration amplification factor of the structure under the TOM wave is 2 times that under the El-Centro wave, while the maximum displacement response of the structure under the TOM wave is 4.4 times that under the El-Centro wave. Long-period ground motions show greater influences on displacement responses than acceleration responses for super high-rise building structures.

3) The input energy of TOM wave is mainly distributed between 4 and 10 s, and the fundamental natural period of the prototype structure is about 9 s, so it is very possible to run into resonance response. The distributions of structural damages and maximum inter-storey drift angles under the TOM wave are both located in the upper part, especially at the 7th and 8th zones. Most inelastic damage occurs at the upper 1/3 part of the super high-rise building when being subjected to long-period ground motions.

Acknowledgement

The present work is support by the National Natural Science Foundation of China (No. 50978198) and the Ministry of Science and Technology of China (No. SLDRCE08-B-03). These supports are greatly appreciated.

The shaking table test is a supplementary test. The authors would like to thank Prof. LU Xi-lin (Tongji University), Prof. LU Wen-sheng (Tongji University) and Prof. ZHAO Bin (Tongji University) for their kind help during the test.

References

[1] KAGAWA T, ZHAO B, MIYAKOSHI K, IRIKURA K. Modeling of 3D basin structures for seismic wave simulations based on available information on the target area: Case study of the Osaka Basin, Japan [J]. Bulletin of Seismological Society of America, 2004, 94(4): 1353−1368.

[2] TAKEWAKI I, FUJITA K. Earthquake input energy to tall and base-isolated buildings in time and frequency dual domains [J]. The Structural Design of Tall and Special Buildings, 2009, 18(6): 589−606.

[3] LI Chun-feng, ZHANG Yang. Urgency of the study of long-period ground motion [J]. Seismological and Geomagnetic Observation and Research, 2006, 27(3): 1−8. (in Chinese)

[4] LIANG Xing-wen, DONG Zhen-ping, WANG Ying-sheng, DENG Ming-ke. Damage to tall buildings in areas with large epicentral distance during M8.0 Wenchuan earthquake [J]. Journal of Earthquake Engineering and Engineering Vibration, 2009, 29(1): 24−31. (in Chinese)

[5] TAKEWAKI I, MURAKAMI S, FUJITA K, YOSHITOMI S, TSUJI M. The 2011 off the Pacific coast of Tohoku earthquake and response of high-rise buildings under long-period ground motions [J]. Soil Dynamics and Earthquake Engineering, 2011, 31(11): 1511−1528.

[6] IWAKI A, IWATA T. Validation of 3-D basin structure models for long-period ground motion simulation in the Osaka Basin, western Japan [J]. Earthquake Science, 2008, 12(2): 197−215.

[7] CHAVEZ-GARCIA F J, PEDOTTI G, HATZFEID D, BARD P Y. An experimental study of site effects near Thessalonica (Northern Greece) [J]. Bulletin of Seismological Society of America, 1990, 80(4): 784−806.

[8] KOKETSU K, MIYAKE H. A seismological overview of long-period ground motion [J]. Journal of Seismology, 2008, 12(2): 133−143.

[9] VUAN A, KLIN P, LAURENZANO G, PRIOLO E. Far-source long-period displacement response spectra in the Po and Venetian plains (Italy) from 3D wavefield simulations [J]. Bulletin of the Seismological Society of America, 2011, 101(3): 1055−1072.

[10] XIE Li-li, ZHOU Yong-nian, HU Cheng-xiang, YU Hai-ying. Characteristics of response spectra of long period earthquake ground motion [J]. Earthquake Engineering and Engineering Vibration, 1990, 10(1): 1−19. (in Chinese)

[11] FUKUWA N, TOBITA J. Key parameters governing the dynamic response of long-period structures [J]. Journal of Seismology, 2008, 12(2): 295−306.

[12] ARIGA T, KANNO Y, TAKEWAKI I. Resonant behavior of base-isolated high-rise buildings under long-period ground motions [J]. The Structural Design of Tall and Special Buildings, 2006, 15(3): 325−338.

[13] CHUNG Y L, NAGAE T, HITAKE T, NAKASHIMA M. Seismic resistance capacity of high-rise buildings subjected to long-period ground motions: E-defense shaking table test [J]. Journal of Structural Engineering, 2010, 136(6): 637−644.

[14] HUANG Yu, YE Wei-min, TANG Yi-qun, CHEN Tian-ling. Characteristic analysis for seismic ground response of soft soils in Shanghai [J]. Chinese Journal of Underground Space and Engineering, 2005, 1(5): 773−778. (in Chinese)

[15] HUANG Yu, YASHIMA A, SAWADA K, ZHANG Feng. A case study of seismic response of earth embankment foundation on liquefiable soils [J]. Journal of Central South University of Technology, 2009, 16(6): 994−1000.

[16] MARTIN P P, SEED H B. One-dimensional dynamic ground response analyses [J]. Journal of Geotechnical Engineering Division ASCE, 1982, 108(7): 935−952.

[17] TAKEWAKI I. Bound of earthquake input energy [J]. Journal of Structural Engineering ASCE, 2004, 130(9): 1289−1297.

[18] Shaking Table Testing Division, Shaking table model test report of Shanghai Tower [R]. Shanghai: State Key Laboratory of Disaster Reduction in Civil Engineering, Tongji University, 2010. (in Chinese)

[19] REZAIFAR O, KABIR M Z, TARIBAKHSH M, TEHRANIA N. Dynamic behavior of 3D-panel single-story system using shaking table testing [J]. Engineering Structures, 2008, 30(2): 318−337.

[20] LU Xin-zheng, YE Lie-ping, MIU Zhi-wei, MA Qian-li, LIN Xu-chang, QU Zhe. Elasto-plastic analysis of buildings against earthquake—theory, model and implementation on ABAQUS, MSC.MARC and SAP2000 [M]. Beijing: Chinese Architecture & Industry Press, 2009: 80−105. (in Chinese)

[21] PRC Ministry of Construction. Code for design of concrete structures GB50010-2002 [S]. Beijing: Chinese Architecture & Industry Press, 2002. (in Chinese)

[22] DING Jie-min, CHAO S, ZHAO Xin, WU Hong-lei. Critical issues of structural analysis for the Shanghai Tower project [J]. Journal of Building Structures, 2010, 31(6): 122−131. (in Chinese)

[23] LU Xi-lin, ZHOU Ying, LU Weng-sheng. Shaking table model test and numerical analysis of a complex high-rise building [J]. The Structural Design of Tall and Special Buildings, 2007, 16(2): 131−164.

(Edited by HE Yun-bin)